Scientia Iranica B (2020) 27(4), 1982–1994

Sharif University of Technology
Scientia Iranica
Transactions B: Mechanical Engineering
http://scientiairanica.sharif.edu

Pulsed Nd: YAG laser dissimilar welding of Ti/Al_{3105} alloys

A.A. Shehab[a,b], S.K. Sadrnezhaad[c,*], A.K. Mahmoud[a], M.J. Torkamany[d], A.H. Kokabi[c], and M. Fakouri Hasanabadi[c]

a. *Department of Material Engineering, College of Engineering, University of Diyala, Diyala, Iraq.*
b. *Institute of Laser for Postgraduate Studies, University of Baghdad, Baghdad, Iraq.*
c. *Department of Materials Science and Engineering, Sharif University of Technology, Tehran, Iran.*
d. *Iranian National Center for Laser Science and Technology (INLC), Tehran, Iran.*

Received 11 November 2018; received in revised form 28 January 2019; accepted 22 April 2019

KEYWORDS
Welding;
Strip;
Joining;
Lasers;
Lapping;
Aluminum;
Titanium;
Keyhole.

Abstract. Overlapped strips of titanium grade 2 and aluminum 3105-O alloy were welded together under an innovative spot-like pulse laser procedure. The tactile seam tracking on ring paths yielded reliable weld fit-up of 1 and 0.5 mm thickness strips. Since the welding parameters of Ti-Al were narrow, three welding speeds of 4, 5, and 6.67 $mm.s^{-1}$ were chosen for the pretest conditions. The microstructural investigations showed that intermetallic compound Ti_3Al formed in the Ti-rich fusion zone. Cracks formed in the Al-rich fusion zone as a result of $TiAl_3$ precipitation. Dimple fracture occurred at 6.67 $mm.s^{-1}$ welding speed. Longer mixing time at Ti-Al interface occurred at lower welding speeds of 4 and 5 $mm.s^{-1}$, which led to the formation of thicker intermetallic compounds and more massive crack generation. It also increased the hardness of the fusion zone and resulted in brittle fracture type during the tensile test. The highest strength was achieved with a welding speed of 4 $mm.s^{-1}$, which was a result of more massive weld nugget and lower porosity.

© 2020 Sharif University of Technology. All rights reserved.

1. Introduction

Research on welding of titanium to aluminum is considered significant for aerospace, automotive, and shipbuilding industries [1–6]. Due to low density, high strength, superior toughness, and resistance to corrosion, previous authors have defined any advancement in this field as substantial to the growth of new technologies [1,7]. The high ductility makes Al 3105-O an excellent candidate to replace aluminum 3003, which is used in the airplane cabin fins by receiving hot or cold fluid from carrying pipes made of titanium grade 2.

The difference in the lattice structure and thermophysical properties of Al and Ti makes their joining process a real challenge, especially by conventional fusion welding methods. From the Ti-Al equilibrium diagram, one can deduce that Al does not allow dissolution of much Ti, while titanium can form a Ti-rich solid solution of up to $\sim$ 12 atom% Al [8]. Negative enthalpies of dissolution [9] help fast fusion of the mixture, while various intermetallic compounds (IMCs) like $TiAl_{3.3}$, TiAl, Ti_5Al_{11}, Ti_9Al_{23}, and $Ti_{3.3}Al$ can also be formed [10]. Intermediate materials have introduced, however, a possible solution to the IMCs problem in the dissimilar welding practices [11].

Laser welding of alloys provides many advantages

*. *Corresponding author.*
E-mail address: sadrnezh@sharif.edu (S.K. Sadrnezhaad)

doi: 10.24200/sci.2019.52217.2600

over conventional techniques, such as great precision, super speed, great flexibility, high quality, and low distortion [12–20]. Majumdar et al. [9] stated that it would be impossible to obtain Al contents below 20 atom% in the Al-Ti Mixing Zone (MZ) and make crack-free weld via the combination of any process parameters during Carbon Dioxide (CO_2) laser welding of Ti-6Al-4V and AlMg0.9Si. They observed that sandwiching of Nb plate between Ti and Al sheets would keep 11 atom% Al in the FZ and form TiNb solid solution with a crack-free joint.

Chen et al. [18] reported that the formation of IMCs inside Ti weld could be suppressed by lowering the laser power or decreasing the welding speed during CO2 laser welding in overlap titanium-on-aluminum configuration. Kreimeyer et al. [19] reported that the thickness of IMCs mainly depended on the energy input per unit length. They obtained IMC thicknesses less than 2 μm in CO_2 laser welding, where crack propagation from the Al HAZ towards IMCs resulted in ductile fracture of the weld. Tomashchuk et al. [20] studied the effect of beam energy and beam offset on the weld morphology, microstructure, and mechanical properties. They observed the formation of a wide contact interface (90–300 μm) rich in Al_3Ti phase when the laser beam was located at the center or AA5754 side. Maximal joint strength was obtained when shifting the laser beam to AA5754 side due to the formation of a thin interface (< 20 μm) composed mostly of TiAl. Chelladurai et al. [21] studied the effect of pulsed Nd: YAG laser energy on the disposition of conduction, transition, penetration, and keyhole. Grain refinement by rapid cooling and hard ceramic particles produced by in-situ reactions may also lead to increase in microhardness [22]. Chen et al. [23] reported on the residual stress induction caused by the difference between thermal expansion coefficients of 5A06 Al and Ti-6Al-4V, leading to crack initiation and its propagation within the reaction layer during the welding brazing process. They expected that lamellas, cellular, and club-shape interfacial layers were responsible for enhancing the mechanical property of the joints by preventing crack initiation and propagation.

Some authors have changed the length of Al-Ti interface by changing joint configuration via making a groove [23] or a chamfer [24] on the welding materials. Vaidya et al. [24] reported joint modification via chamfering of Ti-6Al-4V to the AA6056 alloy by laser, which reduced $TiAl_3$ formation. They observed increase in fatigue crack propagation with the cooling rate, which resulted in complete transgranular fracture of FZ next to the weld interface. From their results, one could conclude that grooving would be more helpful than making a chamfer.

In the present study, a tactile seam tracking system is designed for pulse welding of titanium grade 2 to aluminum 3105-O alloy by a high-energy laser instrument. Increase in the length of joining of very dissimilar materials (Ti-Al) at the interface via utilizing a ring weld path assists the achievement of sufficient joint strength and results in efficient use of the limited area allowable for welding maneuver. Effect of welding speed on microstructure and mechanical properties of the joint is discussed in the paper.

2. Materials and methods

Commercial sheets of Ti (G2) and 3105-O Al were used for welding tests. The chemical composition of the materials was analyzed by using atomic absorption instrument GBC model: Avanta PM, Australia. A SANTAM model STM-20 universal testing machine was used to determine mechanical properties of the base metal sheet according to the standard ASTM-E8, sub-size tensile specimen (Figure 1), by taking the average of three tests. The exact grade of the materials was confirmed by comparing the experimentally determined chemical composition and mechanical properties with the standards in [25]. Chemical compositions and properties of the materials used are given in Tables 1, 2, and 3.

The thickness of Ti (G2) was 1 mm and of Al 3105-O was 0.5 mm. Both metals were cut into 40×5 mm^2 rectangle strips. The surfaces of the strips were degreased by acetone, polished with emery papers, cleaned with 6–10% NaOH alkaline solution for 5 min, and then rinsed with tap water followed by 30% HNO_3 + 3% H_2SO_4 acid solution for 3 min. Ti strips were etched for 5 min with 20% HNO_3+ 5% HF acid solution and then, wiped and rinsed with ethanol and tap water, ten min before welding test. The strips were overlapped for 5 mm and welded in a circular path by overlapping repeated laser pulses, as shown in Figure 2.

Nd: YAG laser apparatus (Model IQL-10) with normal power of 400 W produced standard square-

Figure 1. SANTAM universal testing machine and Al sub-size tensile specimen.

Table 1. Chemical composition of the raw materials in wt%.

Alloy	C	Mn	Cr	Zn	O	Mg	Cu	Fe	Al	Ti
Al 3105-O	—	0.500	0.008	0.060	—	0.500	0.090	0.610	Bal.	—
Ti (G2)	0.080	—	—	—	0.200	—	—	0.080	—	Bal.

Table 2. Mechanical properties of the raw materials.

Alloy	Yield stress (MPa)	Ultimate tensile strength (MPa)	Elongation (%)	Hardness (HV)
Al 3105-O	55	122	24	45
Ti (G2)	275	344	28	125

Table 3. Thermophysical properties of the materials used [22].

Alloy	Thermal conductivity ($W.m^{-1}.K^{-1}$)	Density ($g.cm^{-3}$)	Melting point (°C)	Thermal expansion coefficient ($K^{-1}.\mu m.m^{-1}$)
Al 3105-O	173.0	2.7	660.0	23.6
Ti (G2)	16.4	4.5	1665.0	9.4

shape pulses of 1–1000 Hz frequency, 2–20 ms duration, and 0–40 J energy. The focal length of the focusing optical system was 75 mm, which created spots of ∼250 μm in size. A movable XYZ table moved the clamping device under laser head of 0.05 mm positioning precision. Setup of the welding system was as demonstrated in Figure 2. A coaxial nozzle around the laser beam blew the shielding gas (argon of 99.999% purity) at the rate of 20 $L.min^{-1}$ to top of the weld line.

For tension tests, the cross-head speed of SANTAM testing machine was 5 $mm.min^{-1}$. Three measurements were done for each data point. After welding, the samples were wire-cut from near the welding zone. Grinding with abrasive silicon carbide papers of 600, 800, 1200, 2000, and 3000 $grain.in^{-2}$ and subsequent polishing of the samples with three different grain sizes of wet alumina powder on felt wheels were performed.

For microstructural examination of the weld zone, etching with fresh Kroll reagent was done for 30 s. Optical microscope, Scanning Electron Microscope (SEM), and TESCAN MIRA 3 (Czech) equipped with energy dispersive X-ray spectrometry (EDS) inspected the appearance, geometry, microstructure, and fracture zone of the joints. To investigate phase formation at fracture surfaces, X-Ray Diffraction (XRD) with PAN, Model X′Pertequipped with PIXcel detector, and X′Pert high score plus (V.3) software were used. The metal target was Cu, step size was 2θ, and diffraction angle was 15° at the start and 80° at the end. Buehler model MMT1, USA, determined the Vickers microhardness values. Loading force was 25 g, which was applied for 25 s. Average of three measurements was recorded for different locations: BM, HAZ, and FZ for each side of the joints.

3. Results and discussion

Seam welding procedure of ring path performed with pulse laser spot method provided the premium solution to the problem of high quality Ti-Al joint achievement. Applying conventional laser welding with all combinations of pulse duration and peak power, whether single or multi-pulse and at the same or different positions, did not give enough strength in the welded couple so that the sample could not withstand the pullout force for its removal from the clamping device. However, overlapping pulses of the ring path resulted in a shear strength of around 10 MPa, which depended on the welding speed.

Due to its significant effect on the amount of heat input and the interaction period between the heat source (laser beam) and the weld metal, variation of welding speed had more significant effect on the bead depth than on its width [26,27]. The welding speed has thus a significant effect on the strength of the weld. Another essential factor of seam welding was pulse overlapping, which strongly affected the weld quality by efficient heating and continuous penetration of the substances. The variation of the welding speed affected pulse overlapping and uniform pool formation. Based on pretest experiments, the welding parameters were chosen for the work as listed in Table 4.

3.1. Weld appearance

Figure 3 shows top (Ti) view of the welded samples 1 to 3. The appearance of the surfaces shows the effect of the welding speed on weld zones of the samples. Figure 4 depicts the effect of the speed of welding on the diameter of the weld zone viewed from the top. It shows that lower speed results in a larger weld zone.

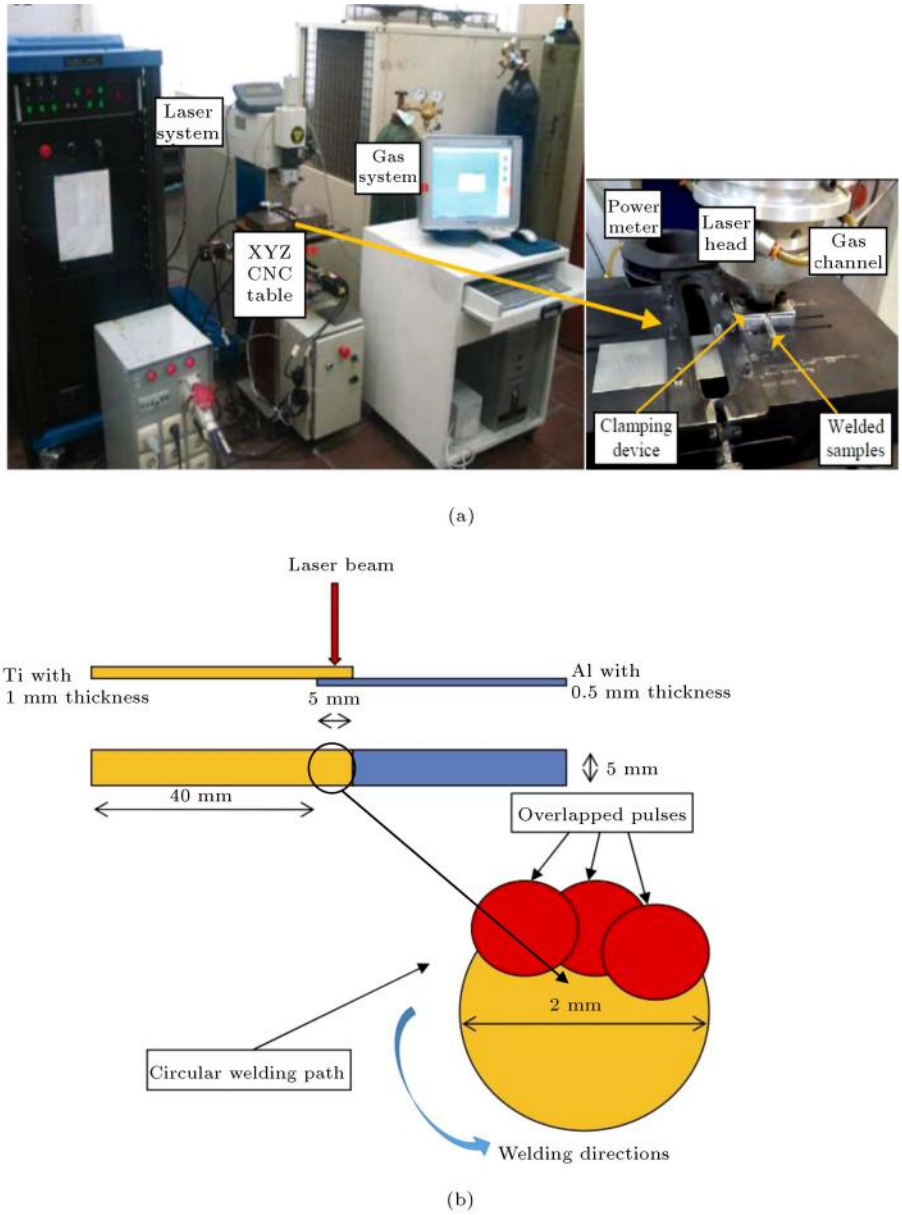

Figure 2. Laser welding of Ti-Al strips: (a) Equipment and (b) setup geometry.

This effect is attributed to the higher energy input due to the longer beam incidence, which leads to a broader base metal pool and a greater weld diameter (3.4 mm for 4 mm.s^{-1} welding speed) (see Figure 3(a)).

Getting a perfect joint between the welded partners requires a reasonable level of pulse overlapping in a way that overlapping of the succeeding pulses leads to a continuous seam weld as observable in Figure 5(a).

Table 4. Values selected for the best welding performance.

Sample no.	Pulse energy E_{pulse} (J)	Pulse duration T (ms)	Welding speed V (mm.s^{-1})	Peak power (kW)	Argon gas flow rate (L.min^{-1})	Pulse frequency f (HZ)	Overlapping factor (%)	Average energy input (J.mm^{-2})
1	11	6	4.00	1.83	20	20	76	137.5
2	11	6	5.00	1.83	20	20	70	110.0
3	11	6	6.67	1.83	20	20	60	82.4

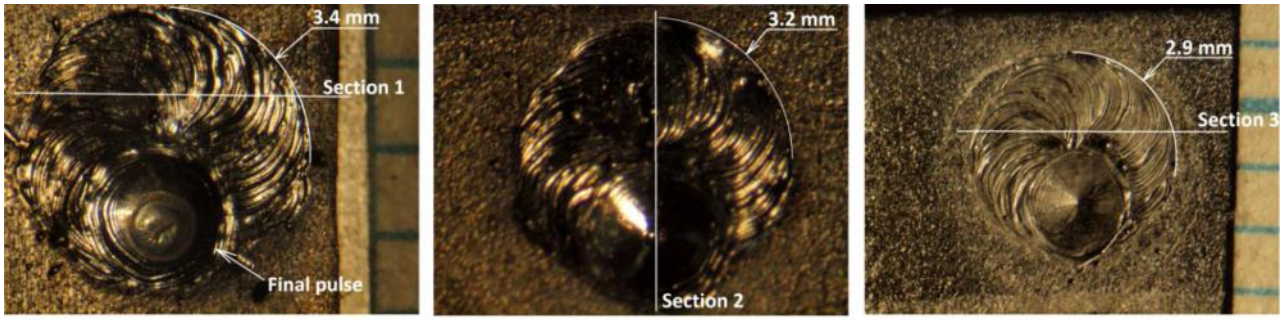

Figure 3. Appearance of the top surface of Ti-Al laser welded couple with various welding speeds: (a) 4, (b) 5, and (c) 6.67 mm.s^{-1}.

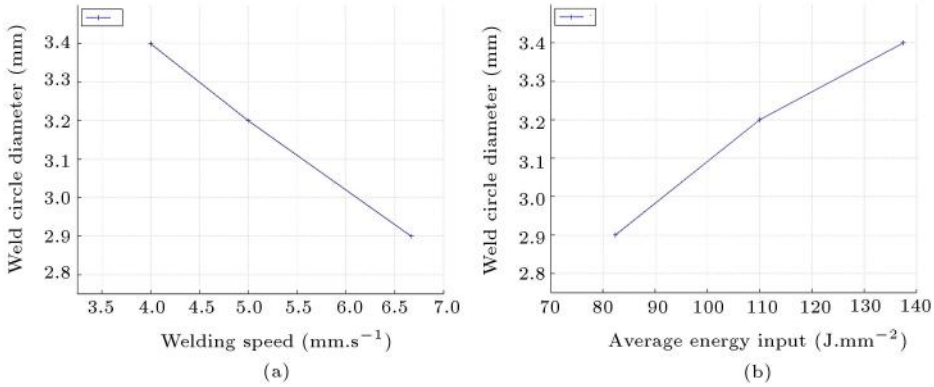

Figure 4. Diameter of the weld zone (mm) vs. (a) Laser welding speed (mm.s^{-1}) and (b) energy input (J.mm^{-2}).

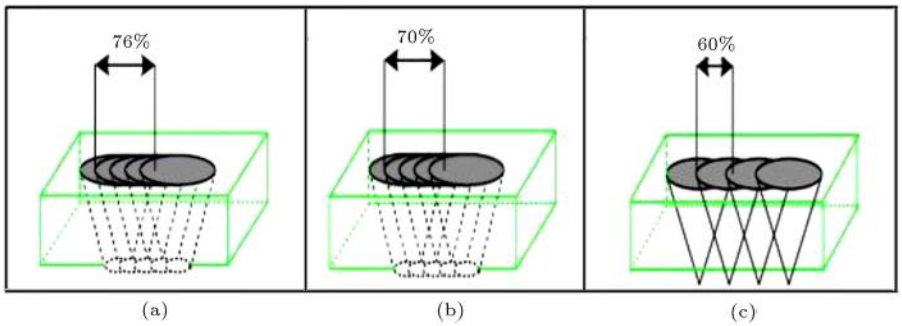

Figure 5. Surface and depth of the keyhole affected by laser beam overlapping (Q_f) of (a) 76%, (b) 70%, and (c) 60%.

Overlapping factor (O_f) is defined as [28]:

$$O_f(\%) = \frac{1-(V/f)}{S+(V\times T)} \times 100, \tag{1}$$

where V is the welding speed, f is laser frequency, T is pulse duration, and S refers to the laser spot size on work-piece that was 0.8 mm throughout our tests. Figure 5 depicts the effect of laser beam overlapping on surface area and keyhole depth. It can be seen that at the welding speed of 6.67 mm.s^{-1} (60% overlapping), the distance between the keyhole roots is longer than that between the other welds being inversely proportional to the overlapping factor Q_f.

By insertion of the test values, i.e. pulse frequency = 20 Hz, $T = 6$ ms, and $S = 0.8$ mm, into Eq. (1), the respective O_f factor became 60, 70, and 76% for the welding speeds of 6.67, 5, and 4 mm.s^{-1}, respectively. Eq. (2) gives the average energy input per unit area (E_a) [29]:

$$E_a = \frac{E_{pulse} \times pulse\ frequency}{\frac{S}{2}} \times V. \tag{2}$$

Decreasing the welding speed (i.e., increasing the overlapping factor O_f) leads to a significant energy effect from the earlier pulse and the severe interaction of the next laser pulse with the metal, which results in

the change of the conical appearance of the welding zone (keyhole shape) to cylindrical. This change causes more efficient energy absorption and more ejection of energy through the generated keyhole ending up with a larger melt volume. This hypothesized mechanism also agrees well with the results of the earlier investigations [28–32].

Experimental results show that a welding speed of 4 mm.s^{-1} (76% overlapping) results in a deeper penetration (342 μm) than the higher welding speed of 6.67 mm.s^{-1} (60% overlapping) (184 μm) does. This is due to the input of a stronger focal energy at the lower speed, which is in agreement with the mechanism described by the previous authors [18,33]. In the last pulse region (end spot of the ring welding path), there are three pulses which collide with the same place before the laser power-supply turns off and the moving head wholly stops. A big circular dip forms at this position at all three speeds, as seen in Figure 3.

Because of higher energy absorption and penetration continuity, overlapping has a powerful influence on the welding efficiency, as indicated by previous researchers [34]. Figure 6 shows the shape of the fused area at the bottom of the Ti strip for different overlapping pulses (O_f) of (a) 76, (b) 70, and (c) 60%. Incomplete fusion appears in some zones of the strip with 60% overlapping. The porosities that form in the 60% O_f sample do not allow energy response for the formation of a continuous complete weld. Multiple pulses of higher overlapping at lower welding speeds can improve the joint, as observed in Figure 6(a) and (c). Decrease in porosity due to the reduction in the welding speed indicates higher heat input rate, which induces an upward flow of the melt to give a chance to the gas bubbles to ascend through the molten pool for their eventual egress, as observed in Figure 6. This mechanism seems to prove a narrow window for the influence of the welding parameters.

Figure 7 presents images of the cross sections 1, 2, and 3 of the weld zone (labeled in Figure 3). This figure shows that penetration depth (for the ordinary overlapped pulses) increases with lowering of the welding speed. This increase is due to the higher energy input that leads to a deeper melt pool, which agrees well with the results of a previous investigation [18]. Figure 7 shows small porosities near fusion boundaries. These porosities are attributed to gases, which are soluble in the liquid melt but insoluble in the solid phase. High solidification rate of the molten pool does not allow the entrapped gases to escape. Initial sources of gas are interfacial and shielding moisture. Effects of both regular and last pulses on the geometry of the weld bead are seen in Figure 7. Due to the extensive energy input of the last three pulses, broader and deeper weld pool forms at the final stage of our circular welding process.

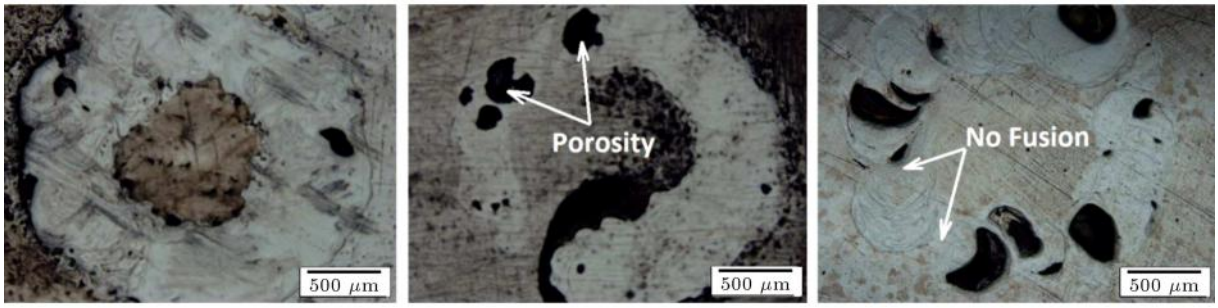

Figure 6. Images of fused areas at the bottom of Ti sheet for different overlapping factor (O_f) values: (a) 76%, (b) 70%, and (c) 60%.

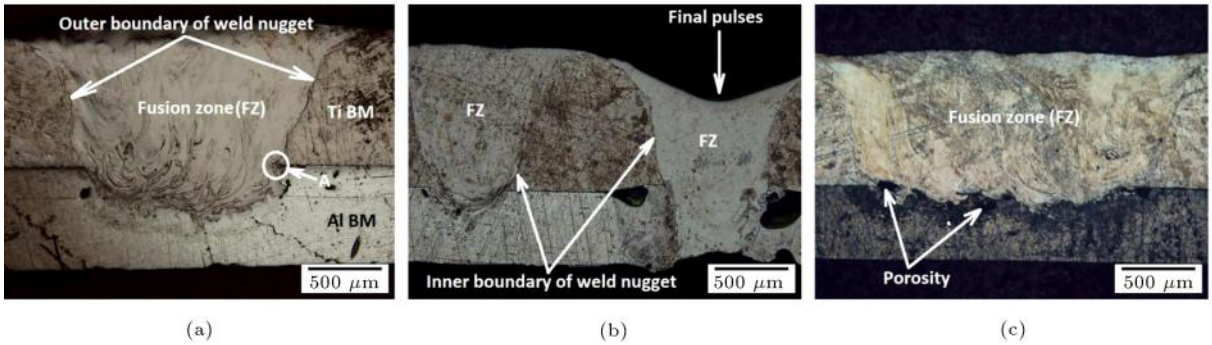

Figure 7. Cross sections of the weld strips highlighted in Figure 3: (a) Section 1, (b) Section 2, and (c) Section 3.

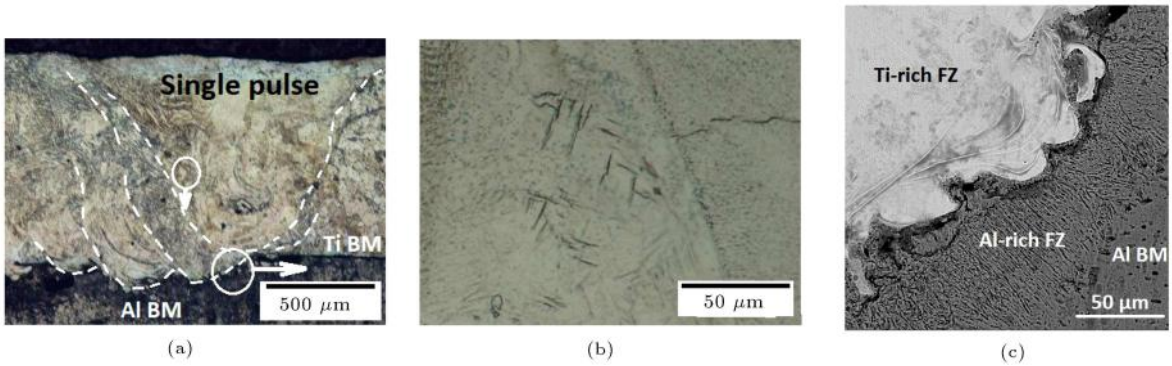

Figure 8. Microstructure of sample 3 ($V = 6.67$ mm.s^{-1}): (a) Serrated α grains in the fusion zone of a single pulse, (b) acicular α' martensite in Ti fusion zone, and (c) Al base metal/fusion zone interface.

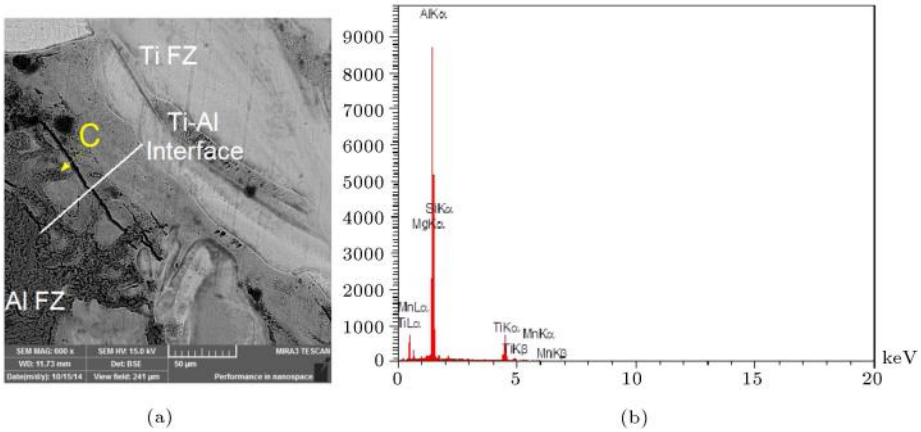

Figure 9. Cracks near the Ti-Al interface at the welding speed of 5 mm.s^{-1}: (a) Scanning Electron Microscope (SEM) image and (b) Energy Dispersive X-ray Spectrometry (EDS) result.

3.2. Weld microstructure

Figure 8 illustrates the microstructure of sample 1. The microstructure of Ti (G2) base metal has equiaxed α grains of uniform size. Energy input during welding generates coarse equiaxed grains in the HAZ and serrated α grains in some areas of the FZ, where heat transfer is along transversal and axial directions. Presence of fine equiaxed grains in the HAZ region next to the molten boundary is due to rapid cooling of the weld metal.

The high cooling rate of more than 104 K.s^{-1} during laser welding [12] is responsible for the formation of the martensite-like structure seen in Figure 8(b). This process modifies the shape and size of the grains in the FZ of Figure 8(a). Ti-α grains in FZ region (bigger than the base metal) are observable in this figure.

Figure 8(c) shows cellular grains grown at the boundary between Al BM and Ti-rich FZ, which is high-rate directional heat ejection towards the Al BM. The high thermal conductivity of Al results in rapid heat transfer and fast cooling in this region.

All areas next to the connection interface consist of columnar grains that are also parallel to the cooling direction. Grains become smaller from Al alloy towards the connection interface owing to the cooling rate enhancement in this direction.

At higher welding speeds of 5 and 6.67 mm.s^{-1}, there is no time for full melt-down of titanium. Ti-Al inter-diffusion at these speeds is also slow due to energy shortage and lack of time. Thus, rapid cooling results in the creation of aluminum-rich IMCs ($TiAl_3$ and/or $TiAl_2$) near Al FZ, which is consistent with the equilibrium phase diagram [8]. Susceptibility to solidification cracking of the weld near Al FZ, hence, increases at higher welding rates. Figure 9(a) shows part of Al-Ti interface for 5 mm.s^{-1} welding speed. Cracks are observable near the Al side of the connection. EDS point scan of point C (see Figure 9(b)) indicates the formation of $TiAl_3$ (22 atom% Ti and 77 atom% Al) in the Al FZ region. Partial melt-down of Ti is expected at higher welding speeds near Al fusion zone.

The increase in local hardness of the connection region is due to high values of modulus of elasticity of $TiAl_3$ in addition to the residual stresses, which exist in the connection [28]. Due to the large difference between thermal conductivity of the Al alloy (173 W.m.K^{-1}) and Ti (16.4 W.m.K^{-1}) [24] as well as low ductility of

$TiAl_3$, the high thermal gradient existing across the connection between the fusion zone and the Al re-solidified alloy can lead to high residual stress near the connection. Since $TiAl_3$ cannot bear this thermal shock, cracks form in the connection region of the welded samples [9].

3.3. Point scan pattern

Figure 10 shows microstructure of zone A of Figure 7(a) and its adjacent regions. Figure 10(a) shows a high magnification SEM image of zone A. Figure 10 (b), (c), and (d) shows the respective EDS results for points A, B, and C of part (a). Table 5 presents the analysis of these points. It is seen that the weld zone mainly has intermetallic phases of Ti_3Al (at Ti side), $TiAl_3$ (at Ti-Al interface), and Al in FZ near the Ti-Al interface.

Figure 11 shows high-magnification SEM images of point C for welding speeds of 4 and 6.67 $mm.s^{-1}$. EDS analyses show the disposition of $TiAl_3$ in both cases. Crack formation occurs at the welding speed of 4 $mm.s^{-1}$ (Figure 11(b)), while it is not observable at the speed of 6.67 $mm.s^{-1}$ (Figure 11(a)). This could have resulted from considerable heat input, low weld speed, small cooling rate, and prolonged Ti-Al mixing, which results in enormous amounts of IMCs ($TiAl_3$) at 4 $mm.s^{-1}$. This compound is very brittle and unable

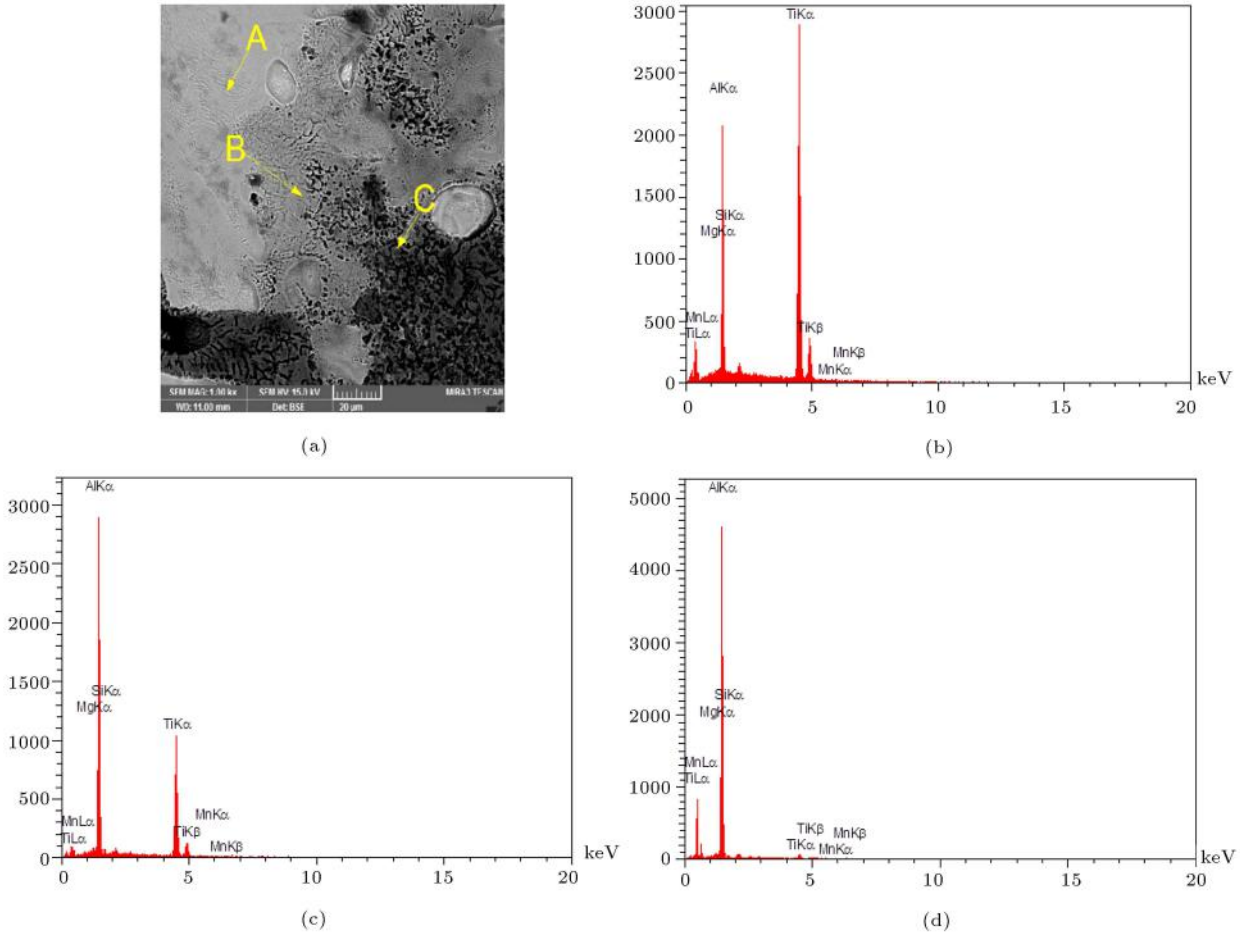

Figure 10. Microstructures of zone A in Figure 7(a) and its adjacent regions: (a) Scanning Electron Microscope (SEM) image for zone A and (b, c, and d) Energy Dispersive X-ray Spectrometry (EDS) patterns of points A, B, and C in part (a), respectively.

Table 5. Weight and atomic percentages of Al and Ti at points A, B, and C in Figure 10(a).

	Ti		Al			
Point	**wt.%**	**atom%**	**wt%**	**atom%**	**Ti_xAl_y**	**Comment**
A	89.3	82.6	10.3	16.9	Ti_3Al	Mixed (αTi + IMCs Ti_3Al)
B	69	56	29.9	43	TiAl	IMCs
C	7.5	4	89.8	93	$TiAl_3$	IMCs

Table 6. Effect of welding speed on mechanical properties of the joint.

Welding speed ($mm.s^{-1}$)	Shear force at the yielding point (N)	Shear strength (N)	Length extension (mm)
4.00	30	264	1.66
5.00	39	256	1.45
6.67	62	244	1.05

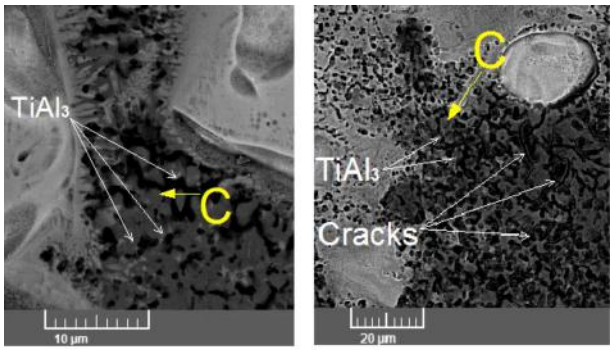

Figure 11. Scanning Electron Microscope (SEM) image nearby point C at the welding speeds of (a) 6.67 and (b) 4 $mm.s^{-1}$.

to withstand the generated thermal shock and hence cracks, as observed in Figure 11(b).

3.4. Mechanical behavior

Mechanical properties of the joint are defined in terms of both tensile and shear strength and microhardness.

3.4.1. Shear strength of the joint

Table 6 represents the shear force and length extension of the samples at various welding speeds. Upshot effect of the laser pulses shows 60% overlap at 6.67 $mm.s^{-1}$, 70% at 5 $mm.s^{-1}$, and 76% at 4 $mm.s^{-1}$. At the higher welding speed of 6.67 $mm.s^{-1}$, the greatest shear force is lower (244 N) due to the smaller O_f; while at the lower welding speed of 4 $mm.s^{-1}$, the greatest shear force is higher (264 N). Incomplete fusion in the areas between the overlapping pulses at the bottom of the Ti sheet at lower overlap percentages is the cause of this effect (see Figure 6(c)). Nonfused areas combined with residual stresses of shear loads can cause crack initiation [23]. Porosities present at the Ti-Al interface (see Figures 6(c) and 7(c)) can also have a negative effect on the joint strength.

Figure 12(a) and (d) presents the optical and SEM images of the samples fractured at the welding speed of 6.67 $mm.s^{-1}$. It shows that fracture starts from the welding zone. This is due to the debonding of the unfinished fusion areas together with

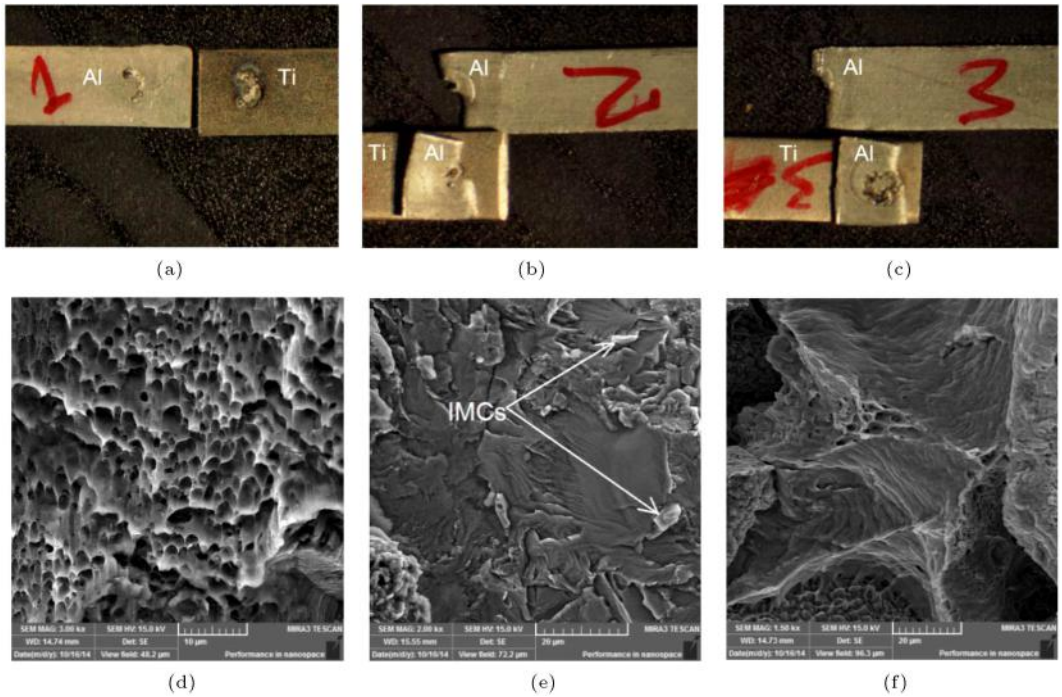

Figure 12. Optical (a, b, and c) and SEM (d, e, and f) images of the samples fractured under shear load at the welding speeds of: (a and d) 6.67, (b and e) 5, and (c and f) 4 $mm.s^{-1}$.

porosity effects. SEM images of the fractured surfaces show a honeycomb-like structure that indicates ductile fracture [19]. The reason is smaller thickness of IMCs formed at the Ti-Al interface at the welding speed of 6.67 mm.s^{-1} (high cooling rate), where less time is available for mixing Ti with Al. Higher shear force (264 N) at the lower welding speed of 4 mm.s^{-1} leads to deeper penetration of titanium into aluminum and larger width of joining due to higher heat input. The wider melted area (3.77 mm^2) at Ti-Al interface (average of three measurements) besides lower porosity levels of sample 3 gives the higher shear force value of 264 N with longer extension during the tensile test (see Table 6, Figure 6(a)).

The joint strength in lap joint design mainly depends on the melted area of the connection and the strength of the welded sheets [35,36]. Dividing the shear force (264 N) by surface area (3.77 mm^2) gives the shear stress at the interface. The result is the shear stress of 70 MPa.

Figure 12(b) and (c) presents the optical images of the fractured samples 2 and 3. Images indicate breaking of the sample from Al FZ, which is very close to the Ti-Al interface. As a result, one can infer that the cracks form in the IMC zone. This is due to the high heat input (see Figures 9(a) and 11(b)), which agrees with the literature [37]. SEM images of the fractured surfaces of samples 2 and 3 are also presented in Figure 12(e) and (f). Figure 12 also shows locations of cleavage fracture. They indicate a brittle fracture [38].

XRD patterns of the fracture surface of sample 2 (welding speed: 5 mm.s^{-1}) in Figure 12(b) are given in Figure 13. The small XRD peaks belonging to $TiAl_3$ (Figure 12(e)) show IMCs $TiAl_3$ formation.

Figure 14 compares the values of (1) joint shear stress at the welding speed of 4 mm.s^{-1} (76% pulses overlap), (2) aluminum base metal shear stress, and (3) aluminum base metal tensile stress. In the joints with dissimilar metals, it is more logical to compare the value of the shear stress of the joint (70 MPa) with the shear stress of the lower-strength base metal, aluminum (82 MPa) here. Accordingly, the high joint shear strength of 85% with respect to the base metal is obtained.

3.4.2. Microhardness of the joint

Vickers microhardness numbers (average of three measurements) for locations BM, HAZ, and FZ of the welded samples are marked in Figure 15. On the Ti side, microhardness increases from Ti HAZ towards the FZ region. A drastic difference between Ti BM (125 HV) and Ti FZ (317 HV) is also observed. Acicular α-martensite, which forms due to thermal-cycling by the laser heat and the next quench, seems responsible for this difference, as also stated in [12]. The hardening effect observed in the Ti-Al dissimilar

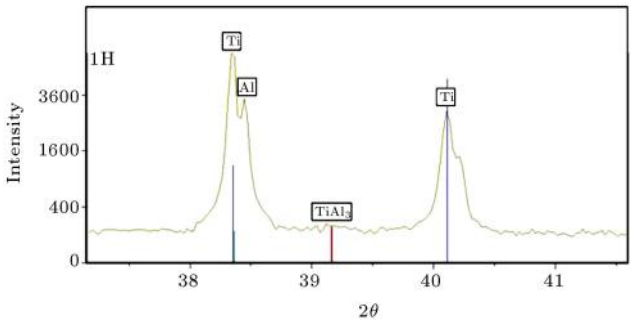

Figure 13. X-Ray Diffraction (XRD) patterns at the fracture interface of Ti shown in Figure 12(e).

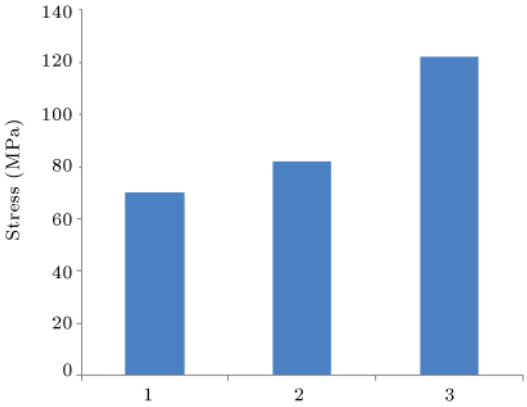

Figure 14. Values of (1) the shear stress for the joint welded at 4 mm.s^{-1} (76% pulses overlap), (2) the shear stress for the Al base metal, and (3) the tensile stress for Al base metal.

weld interface is attributed to the IMCs formed at the hardened locations, as observed in Figure 15. It is also observed that the thickness of the IMCs changes with the welding speed. Different IMCs form at different cooling rates and times from the beginning of Ti-Al mixing. However, the increase in IMCs thickness, which relates to the decrease in the welding speed, leads to increase in the joint hardness, as seen in Figure 15(a), (b), and (c). In this figure, 412, 464, and 572 HV represent the maximum hardness value at the Ti-Al mixing zone (MZ) for samples 1, 2, and 3, respectively. Thus, dimple fracture was observed in sample 1 (Figure 12(d)) and brittle cleavage occurred in samples 2 and 3 (Figure 12(e) and (f)).

On the aluminum side of the connection, there is an increase in microhardness values from Al HAZ towards FZ region. The hardness of aluminum at FZ is higher than that at Al BM. The higher hardness is because of high grain growth and coarsening at low cooling rates of Al BM as compared to the Al at FZ. The resulting increase in hardness of the Al at FZ as compared to the corresponding Al at BM (45 HV) is thus logically due to the grain refinement, which results from the high cooling rate of the laser-welded region.

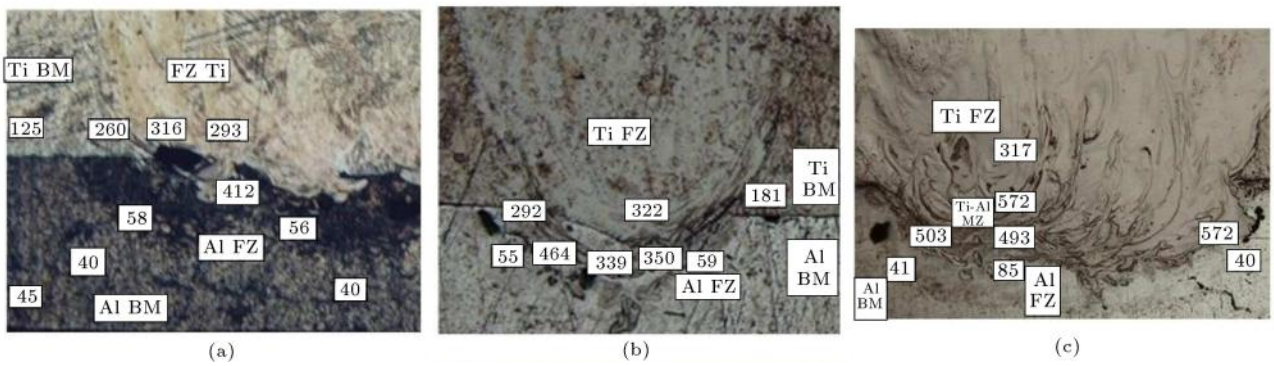

Figure 15. Base Metal (BM), Fusion Zone (FZ), and Mixing Zone (MZ) microhardness measurement locations on the Ti-Al couple welded at the speeds of (a) 6.76, (b) 5, and (c) 4 mm.s^{-1}.

4. Conclusions

Nd: YAG pulsed laser welding of dissimilar 1 mm thick titanium grade 2 strip and 0.5 mm thick aluminum 3105-O alloy belt showed that:

1. The specific spot welding procedure adopted in the present work was an efficient method for making a joint of very different materials, such as Ti-Al joint, over a limited area allowable for welding;
2. Intermetallic compounds (IMCs) Ti_3Al were formed in Ti Fusion Zone (FZ) near the connection. Precipitation of $TiAl_3$ IMCs in Al FZ near the connection resulted in the formation of cracks;
3. Longer mixing time at lower welding speed led to the formation of thicker IMCs, initiation of more cracks, and increase in hardness at the Ti-Al joint;
4. Welding speeds of 5 and 6.67 mm.s^{-1} did not give desirable results due to the diminution of heat input and narrowing of the melt pool. Welding speed of 4 mm.s^{-1} led to larger width of joining of titanium and aluminum with lower porosity. Joint strength rose up to 85% of the base aluminum alloy.

Acknowledgments

The authors would like to thank co-operation of the Institute of Laser for Postgraduate Studies, University of Baghdad, Sharif University of Technology, Iran National Science Foundation, and Iranian National Center for Laser Science and Technology for their help and support of doing this work.

References

1. Möller, F., Grden, M., Thomy, C., and Vollertsen, F. "Combined laser beam welding and brazing process for aluminium titanium hybrid structures", *Phys. Procedia*, **12**(Part 1), pp. 215–223 (2011).
2. Zhu, Z., Lee, K.Y., and Wang, X. "Ultrasonic welding of dissimilar metals, AA6061 and Ti6Al4V", *Int. J. Adv. Manuf. Technol.*, **59**(5–8), pp. 569–574 (2012).
3. Sohn, W.H., Bong, H.H., and Hong, S.H. "Microstructure and bonding mechanism of Al/Ti bonded joint using Al-10Si-1Mg filler metal", *Mater. Sci. Eng. A*, **355**(1–2), pp. 231–240 (2003).
4. Kahraman, N., Gulenc, B., and Findik, F. "Corrosion and mechanical-microstructural aspects of dissimilar joints of Ti-6Al-4V and Al plates", *Int. J. Impact Eng.*, **34**(8), pp. 1423–1432 (2007).
5. Cao, R., Sun, J.H., and Chen, J.H. "Mechanisms of joining aluminium A6061-T6 and titanium Ti-6Al-4V alloys by cold metal transfer technology", *Sci. Technol. Weld. Join.*, **18**(5), pp. 425–433 (2013).
6. Cao, X., Wallace, W., Immarigeon, J.-P., and Poon, C. "Research and progress in laser welding of wrought aluminum alloys. II. Metallurgical microstructures, defects, and mechanical properties", *Mater. Manuf. Process.*, **18**(1), pp. 23–49 (2003).
7. Costa, A., Miranda, R., Quintino, L., and Yapp, D. "Analysis of beam material interaction in welding of titanium with fiber lasers", *Mater. Manuf. Process.*, **22**(7–8), pp. 798–803 (2007).
8. Das, S. "The Al-O-Ti (aluminum-oxygen-titanium) system", *J. Phase Equilibria*, **23**(6), pp. 525–536 (2002).
9. Majumdar, B., Galun, R., Weisheit, A., and Mordike, B.L. "Formation of a crack-free joint between Ti alloy and Al alloy by using a high-power CO2 laser", *J. Mater. Sci.*, **32**(23), pp. 6191–6200 (1997).
10. Wei, S., Li, Y., Wang, J., and Liu, K. "Use of welding-brazing technology on microstructural development of titanium/aluminum dissimilar joints", *Mater. Manuf. Process.*, **29**(8), pp. 961–968 (2014).
11. Mitelea, I., Groza, C., and Craciunescu, C.M. "Pulsed laser processing of dissimilar Ti-6Al-4V and X5CrNi18-10 joints", *Mater. Manuf. Process.*, **29**(8), pp. 975–979 (2014).
12. Katayama, S., *Handbook of Laser Welding Technologies*, 1st Edn., Wood Head Publishing, Cambridge (2013).
13. Pascu, A., Stanciu, E.M., Voiculescu, I., Ţierean, M.H., Roată, I.C., and Ocaña, J.L. "Chemical and

mechanical characterization of AISI 304 and AISI 1010 laser welding", *Mater. Manuf. Process.*, **31**(3), pp. 311–318 (2016).

14. Subashini, L., Prabhakar, K.V.P., Gundakaram, R.C., Ghosh, S., and Padmanabham, G. "Single pass laser-arc hybrid welding of maraging steel thick sections", *Mater. Manuf. Process.*, **31**(16), pp. 2186–2198 (2016).
15. Mirshekari, G.R., Saatchi, A., Kermanpur, A., and Sadrnezhaad, S.K. "Effect of post weld heat treatment on mechanical and corrosion behaviors of NiTi and stainless steel laser-welded wires", *J. Mater. Eng. Perform.*, **25**(6), pp. 2395–2402 (2016).
16. Mirshekari, G.R., Kermanpur, A., Saatchi, A., Sadrnezhaad, S.K., and Soleymani, A.P. "Microstructure, cyclic deformation and corrosion behavior of laser welded NiTi shape memory wires", *J. Mater. Eng. Perform.*, **24**(9), pp. 3356–3364 (2015).
17. Mirshekari, G.R., Saatchi, A., Kermanpur, A., and Sadrnezhaad, S.K. "Laser welding of NiTi shape memory alloy: Comparison of the similar and dissimilar joints to AISI 304 stainless steel", *Opt. Laser Technol.*, **54**, pp. 151–158 (2013).
18. Chen, S., Yang, D., Li, M., Zhang, Y., Huang, J., Yang, J., and Zhao, X. "Laser penetration welding of an overlap titanium-on-aluminum configuration", *Int. J. Adv. Manuf. Technol.*, **87**(9–12), pp. 3069–3079 (2016).
19. Kreimeyer, M., Wagner, F., and Vollertsen, F. "Laser processing of aluminum-titanium-tailored blanks", *Opt. Lasers Eng.*, **43**(9), pp. 1021–1035 (2005).
20. Tomashchuk, I., Sallamand, P., Cicala, E., Peyre, P., and Grevey, D. "Direct keyhole laser welding of aluminum alloy AA5754 to titanium alloy Ti6Al4V", *J. Mater. Process. Technol.*, **217**, pp. 96–104 (2015).
21. Chelladurai, A.M., Gopal, K.A., Murugan, S., Venugopal, S., and Jayakumar, T. "Energy transfer modes in pulsed laser seam welding", *Mater. Manuf. Process.*, **30**(2), pp. 162–168 (2015).
22. Sahu, J.K., Sahoo, C.K., and Masanta, M. "In-Situ TiB2-TiC-Al2O3 composite coating on aluminum by laser surface modification", *Mater. Manuf. Process.*, **30**(6), pp. 736–742 (2015).
23. Chen, Y., Chen, S., and Li, L. "Influence of interfacial reaction layer morphologies on crack initiation and propagation in Ti/Al joint by laser welding-brazing", *Mater. Des.*, **31**(1), pp. 227–233 (2010).
24. Vaidya, W.V., Horstmann, M., Ventzke, V., Petrovski, B., Koçak, M., Kocik, R., and Tempus, G. "Improving interfacial properties of a laser beam welded dissimilar joint of aluminium AA6056 and titanium Ti6Al4V for aeronautical applications", *J. Mater. Sci.*, **45**(22), pp. 6242–6254 (2010).
25. ASM Handbook, *Properties and Selection: Nonferrous Alloys and Special-Purpose Materials*, **2**, ASM International, Geauga County, Ohio, USA (1990).
26. Tadamalle, A.P., Reddy, Y.P., and Ramjee, E. "Influence of laser welding process parameters on weld pool geometry and duty cycle", *Adv. Prod. Eng. Manag.*, **8**(1), pp. 52–60 (2013).
27. Azadi Moghaddam, M., Golmezerji, R., and Kolahan, F. "Simultaneous optimization of joint edge geometry and process parameters in gas metal arc welding using integrated ANN-PSO approach", *Sci. Iran., B*, **24**(1), pp. 260–273 (2017).
28. Torkamany, M.J., Malek Ghaini, F., and Poursalehi, R. "Dissimilar pulsed Nd:YAG laser welding of pure niobium to Ti-6Al-4V", *Mater. Des.*, **53**, pp. 915–920 (2014).
29. Torkamany, M.J., Tahamtan, S., and Sabbaghzadeh, J. "Dissimilar welding of carbon steel to 5754 aluminum alloy by Nd:YAG pulsed laser", *Mater. Des.*, **31**(1), pp. 458–465 (2010).
30. Tzeng, Y.-F. "Process characterisation of pulsed Nd:YAG laser seam welding", *Int. J. Adv. Manuf. Technol.*, **16**(1), pp. 10–18 (2000).
31. Torkamany, M.J., Sabbaghzadeh, J., and Hamedi, M.J. "Effect of laser welding mode on the microstructure and mechanical performance of dissimilar laser spot welds between low carbon and austenitic stainless steels", *Mater. Des.*, **34**, pp. 666–672 (2012).
32. Kim, T., Ha, K.H., and Chu, C.N. "Effects of material combination on laser beam drilling of a metal foil using a cover plate", *Mater. Manuf. Process.*, **32**(6), pp. 631–637 (2017).
33. Kalaiselvan, K., Elango, A., and Nagarajan, N. "Studies on weldment structure in Ti/Al dissimilar metal joints using Laser beam welding", *International Journal of Innovation and Scientific Research*, **21**(2), pp. 301–309 (2016).
34. Torkamany, M.J., Hamedi, M.J., Malek, F., and Sabbaghzadeh, J. "The effect of process parameters on keyhole welding with a 400 W Nd: YAG pulsed laser", *J. Phys. D. Appl. Phys.*, **39**(21), pp. 4563–4567 (2006).
35. Ion, J.C., *Laser Processing of Engineering Materials: Principles, Procedure and Industrial Application*, Elsevier, Oxford, England (2005).
36. Ready, J.F., Farson, D.F., and Feeley, T., *LIA Handbook of Laser Materials Processing*, Springer-Verlag Berlin Heidelberg, Heidelberg, Germany (2001).
37. Chen, S.H., Li, L.Q., and Chen, Y.B. "Interfacial reaction mode and its influence on tensile strength in laser joining Al alloy to Ti alloy", *Mater. Sci. Technol.*, **26**(2), pp. 230–235 (2010).
38. Chen, D.-C., Chang, D.-Y., Chen, F.-H., and Kuo, T.-Y. "Application of ductile fracture criterion for tensile test of zirconium alloy 702", *Sci. Iran.*, **25**(2), pp. 824–829 (2018).

Biographies

Abeer A. Shehab received his BSc in Mechanical Engineering from Baghdad University in 2000 and Higher

Diploma in Mechanical Engineering from Middle Technical University of Baghdad in 2008. Moreover, he received his MSc in 2011 and PhD in 2015 from Baghdad University, Institute of Laser for Postgraduate Studies. During 2014, he was on a research mission at Sharif University of Technology under the supervision of Prof. S.K. Sadrnezhaad. He spent six years as a faculty member of the Mechanical Engineering Department in the College of Engineering, University of Diyala. Then, he moved to the Material Engineering Department of the same university in 2017 as a lecturer in welding and casting processes. His primary interest remains in the field of welding laser material processing (laser welding, laser drilling, laser surface treatments, and laser cutting).

Sayed K. Sadrnezhaad is a distinguished Professor in the Department of Materials Science and Engineering at Sharif University of Technology, Iran. His current interest is in the emerging bio-nano fields of the materials science and engineering discipline. His PhD dates back to 1979 from the Massachusetts Institute of Technology. So far, he has authored and coauthored five books, more than 600 technical papers, and more than 60 patents.

Adel K. Mahmoud is Full Professor of Metallurgical and Mechanical Engineering in the Department of Material Engineering, College of Engineering, University of Diyala, in Iraq. He received BSc, MSc, and PhD degrees in Metallurgical Engineering from the University of Technology of Baghdad in Iraq. Dr. Mahmoud has more than 40 papers published in the proceedings of international conferences and journals in the fields of the materials engineering, laser welding of engineering materials, and nanotechnology. His current research lies in the areas of surface engineering, laser processing of engineering materials, and nanomaterials.

Mohammad Javad Torkamany has a BSc in Applied Physics and an MSc in Atomic and Molecular Physics from the University of Isfahan, and a PhD in Material Engineering from Tarbiat Modares University, which he obtained in 2015. Dr. Torkamany has worked as a researcher in the field of high-power laser welding at the Lulea University of Technology in Sweden. Currently, he is a faculty member of the Iranian National Center for Laser Science and Technology (INLC) working on laser material processing, especially pulsed laser welding, nanoparticle production by pulsed laser ablation in liquids, nonlinear optical properties of laser-synthesized nano, and dissimilar laser welding.

Amir Hossein Kokabi received his BSc in Industrial Metallurgy from Sharif University of Technology in 1970. He was directly accepted as a PhD candidate at University of Strathclyde, Scotland, and received his degree in Welding Metallurgy in 1980. Professor Kokabi is a faculty member of Sharif University of Technology. He has done extensive work and has also written several books in the field of metals, ceramics, and polymers joining as well as material processing using welding technologies.

Masood Fakouri Hasanabadi graduated with BSc in Materials Engineering from Ferdowsi University of Mashhad in 2011 and MSc and PhD in welding from Sharif University of Technology in 2013 and 2018. He worked as a researcher at the Institute of Energy and Climate Research of Forschungszentrum Jülich as well as Renewable Energy Department of Niroo Research Institute for several months from 2016 to 2018. He is currently active in pursuing research on welding and ceramic-metal joining.